



Earlier collapse of Anthropocene ecosystems driven by multiple faster and noisier drivers

Willcock, Simon; Cooper, Gregory; Addy, John; Dearing, John

Nature Sustainability

DOI:

<https://doi.org/10.1038/s41893-023-01157-x>

Published: 22/06/2023

Peer reviewed version

[Cyswllt i'r cyhoeddiad / Link to publication](#)

Dyfyniad o'r fersiwn a gyhoeddwyd / Citation for published version (APA):

Willcock, S., Cooper, G., Addy, J., & Dearing, J. (2023). Earlier collapse of Anthropocene ecosystems driven by multiple faster and noisier drivers. *Nature Sustainability*. <https://doi.org/10.1038/s41893-023-01157-x>

Hawliau Cyffredinol / General rights

Copyright and moral rights for the publications made accessible in the public portal are retained by the authors and/or other copyright owners and it is a condition of accessing publications that users recognise and abide by the legal requirements associated with these rights.

- Users may download and print one copy of any publication from the public portal for the purpose of private study or research.
- You may not further distribute the material or use it for any profit-making activity or commercial gain
- You may freely distribute the URL identifying the publication in the public portal ?

Take down policy

If you believe that this document breaches copyright please contact us providing details, and we will remove access to the work immediately and investigate your claim.

1 **Title:** Earlier collapse of Anthropocene ecosystems driven by multiple faster and noisier drivers

2
3 **Author list:** Simon Willcock^{1,2*}, Gregory S. Cooper^{3,4}, John Addy⁵ and John A. Dearing⁶.

4 **Affiliations:**

- 5 1. Net Zero and Resilient Farming, Rothamsted Research, Harpenden, Hertfordshire, AL5 2JQ,
6 UK. simon.willcock@rothamsted.ac.uk
- 7 2. School of Natural Sciences, Bangor University, Bangor, Gwynedd, LL57 2DG, UK.
- 8 3. Institute for Sustainable Food, University of Sheffield, Western Bank, Sheffield, S10 2TN, UK.
- 9 4. Department of Geography, University of Sheffield, Western Bank, Sheffield, S10 2TN, UK.
10 g.s.cooper@sheffield.ac.uk
- 11 5. Intelligent Data Ecosystems, Rothamsted Research, Harpenden, Hertfordshire, AL5 2JQ UK.
12 john.addy@rothamsted.ac.uk
- 13 6. Geography and Environmental Science, University of Southampton, Southampton, SO17 1BJ,
14 UK. j.dearing@soton.ac.uk

15 * Corresponding author

16
17 **Abstract**

18 A major concern for the world's ecosystems is the possibility of collapse, where landscapes and the
19 societies they support change abruptly. Accelerating stress levels, increasing frequencies of extreme
20 events, and strengthening inter-system connections suggest that conventional modelling approaches
21 based on incremental changes in a single stress may provide poor estimates of the impact of climate
22 and human activities on ecosystems. We conduct experiments on four models that simulate abrupt
23 changes in the Chilika lagoon fishery, the Easter Island community, forest dieback and lake water
24 quality – representing ecosystems with a range of anthropogenic interactions. Collapses occur sooner
25 under increasing levels of primary stress, but additional stresses and/or the inclusion of noise in all
26 four models bring the collapses substantially closer to today by ~38-81%. We discuss the implications
27 for further research and the need for humanity to be vigilant for signs that ecosystems are degrading
28 even more rapidly than previously thought.

29
30 **Key words:** climate change, modelling, regime shift, resilience, stress, tipping point.

31
32 **Main text:**

33
34 For many observers, UK Chief Scientist's John Beddington's argument that the world faced a 'Perfect
35 Storm' of global events by 2030¹ has now become a prescient warning. Recent mention of 'ghastly
36 futures'², 'widespread ecosystem collapse'³, and 'domino effects on sustainability goals'⁴ tap into a
37 growing consensus within some scientific communities that the Earth is rapidly destabilising through
38 'cascades of collapse'⁵. Kareiva and Carranza⁶ even speculate on 'end-of-world' scenarios involving
39 transgressing planetary boundaries (climate, freshwater and ocean acidification), accelerating
40 reinforcing (i.e. positive) feedback mechanisms and multiplicative stresses. Prudent risk management
41 clearly requires consideration of the factors that may lead to these bad-to-worst-case scenarios⁷. Put
42 simply, the choices we make about ecosystems and landscape management can accelerate change
43 unexpectedly.

44
45 The potential for rapid destabilisation of Earth's ecosystems is, in part, supported by observational
46 evidence for increasing rates of change in key drivers and interactions between systems at the global
47 scale (SI-1). For example, despite decreases in global birth rates and increases in renewable energy
48 generation, the general trends of population, greenhouse gas concentrations and economic drivers
49 (such as gross domestic product) are upwards^{8,9} – often with acceleration through the 20th and 21st
50 centuries. Similar non-stationary trends for ecosystem degradation¹⁰ imply that unstable sub-systems
51 are common. Furthermore, there is strong evidence globally for the increased frequency and
52 magnitude of erratic events, such as heatwaves and precipitation extremes¹¹. Examples include the

53 sequence of European summer droughts since 2015¹², fire-promoting phases of the tropical Pacific
54 and Indian ocean variability¹³, and regional flooding¹¹, already implicated in reduced crop yields¹⁴, and
55 increased fatalities and normalised financial costs⁹.

56

57 The increased frequency and magnitude of erratic events is expected to continue throughout the
58 twenty-first century. The IPCC AR6 concludes that “multiple climate hazards will occur simultaneously,
59 and multiple climatic and non-climatic risks will interact, resulting in compounding overall risk and
60 risks cascading across sectors and regions”¹¹. Overall, global warming will increase the frequency of
61 unprecedented extreme events¹¹, raise the probability of compound events¹⁵, and ultimately could
62 combine to make multiple system failures more likely¹⁶. For example, there is a risk that multiple
63 tipping points can be triggered within the Paris Agreement range of 1.5 to 2°C warming, including
64 collapse of the Greenland and West Antarctic ice sheets, die-off of low-latitude coral reefs, and
65 widespread abrupt permafrost thaw¹⁷. These tipping points are contentious and with low likelihood
66 in absolute terms, but with potentially large impacts should they occur. In evaluating models of real
67 world systems, we therefore need to be careful that we capture complex feedback networks and the
68 effects of multiple drivers of change that may act either antagonistically or synergistically^{18–20}.
69 Prompted by these ideas and findings, we use computer simulation models based on four real-world
70 ecosystems to explore how the impacts of multiple growing stresses from human activities, global
71 warming and more interactions between systems could shorten the time left before some of the
72 world’s ecosystems may collapse.

73

74 Intuitively, stronger interactions between systems may be expected to increase the numbers of drivers
75 of any one system, change driver behaviour and generate more system noise. As a result, we would
76 anticipate that higher levels of stress, more drivers and noise may bring forward threshold-dependent
77 changes more quickly. For example, for any particular system (e.g. the Amazon forest) it is possible to
78 envisage a time sequence that starts with one main driver (e.g. deforestation), then multiple drivers
79 (e.g. deforestation plus global warming), more noise through extreme events (e.g. more droughts and
80 wildfires), with additional feedback mechanisms that enhance the drivers (e.g. diminished internal
81 water cycle and more severe droughts). A vortex could therefore emerge, with drivers generating
82 noisier systems as climate variability and the incidence of extreme events increases. Under worst-case
83 scenarios, the circle becomes faster as reinforcing feedbacks accelerate connections or human
84 activities increase stress levels. However, extreme events could also counteract each other (e.g.
85 extreme droughts and extreme rainfall events) and interconnections could also have weakening
86 effects – for example where increased plant growth driven by increased CO₂ is counterbalanced by
87 increased temperatures and droughts. To date, there is limited observational evidence showing that
88 ecosystems have a record of tipping between alternate stable states²¹.

89

90 Ashwin *et al.*'s¹⁹ mathematical tripartite classification of critical transitions includes slow driver
91 bifurcations, rate-induced (fast/cumulative driver) and noise-induced (extreme event) tipping points.
92 However, previous studies tend to focus on each of these categories individually. For example, there
93 is a well-established body of physics and mathematical theory on ‘mean exit times’²², with studies
94 investigating the timing of tipping points in rate-induced^{18–20} or noisy^{19,23,24} systems. However, despite
95 calls for more experimental evidence of the impacts of climate variability and extremes on
96 ecosystems^{25,26}, the relative importance or combined effect of fast drivers, multiple drivers and noisy
97 system drivers on the collapse of real world ecosystems is not known. Critical transitions driven by
98 current pollution forcings such as greenhouse gas emissions²⁷ and nutrient loadings²⁸ are likely to be
99 novel, well beyond the envelope of natural variability. Hence, we avoid the use of the terms critical
100 transition and tipping points, used formally in dynamical systems theory to represent shifts to
101 alternative attractors, and focus on abrupt threshold-dependent changes (ATDCs) that would be
102 perceived by society as the quantitative (e.g. fish stock integrity) and/or qualitative (e.g. ecosystem
103 functions) collapse of a desirable system state^{29,30}.

104

105 We have selected a range of system dynamic models that have been previously used to demonstrate
106 generalisable findings (e.g. with regard to safely overshooting ATDCs²⁷) and can be externally
107 manipulated to simulate internal emergent ATDCs at local and regional scales – as if they were
108 impacted through stronger connections to other systems. Reflecting modern ecosystems, these
109 models show varied anthropogenic interactions, ranging from social-ecological systems with strongly
110 coupled human-nature feedbacks to ecological systems with predominantly one-way interactions
111 where ecosystems are influenced by the external impacts of people. The ability of these models to
112 capture feedback-loops, delays and interactions between components is well established^{31,32}, and has
113 motivated their use in various recent studies of sustainability and resilience^{21,33–35}. Therefore, guided
114 by Ashwin *et al.*'s¹⁹ typology of tipping points, we aim to generalise the dynamics of increasing the
115 numbers of drivers, their rates and variability (as proxies for stronger interactions between systems
116 and noise) on the speed at which ATDCs are reached in four ecosystem dynamics models (Figure 1):
117 Lake Chilika lagoon fishery^{21,33}, Easter Island³⁶, Lake phosphorus^{28,37}, and a modified version of The
118 Hadley Centre Dynamic Global Vegetation Model (TRIFFID) of forest dieback^{27,38}.

119

120 **Results**

121 As described in the Methods, the four models each have a primary (baseline) slow driver (Figure 2:
122 grey boxplots), where linear changes in their trajectories over time can initiate ATDCs in their
123 respective outcome variable (Lake Chilika: fish population; Easter Island: human population; TRIFFID:
124 tree coverage; Lake phosphorus: lake phosphorus concentration). When the strength of the primary
125 slow driver in each model is increased, the modelled systems collapse sooner - as defined by a
126 statistical breakpoint in their temporal trends (see Methods Section 3.2). Increasing the strength of
127 multiple drivers with additional secondary and tertiary drivers further reduces the breakpoint date
128 (Figure 2), with variation around these median responses determined by the relative strength of the
129 additional drivers – with addition of a weak secondary driver bringing forward the start of system
130 collapse substantially less than the addition of a strong secondary driver (Figure S2-1).

131

132 In addition to earlier breakpoint dates, extra drivers can also cause ATDCs at levels where it would be
133 resilient to the primary slow driver in isolation (SI-2). For example, across the 1000 timesteps of the
134 Lake phosphorus model, the system is stable at normalised baseline driver rates up to 0.348 (i.e., Lake
135 phosphorus concentration does not go through a breakpoint; Figure S2-4D). However, the addition of
136 a single secondary driver of normalised strength 0.3 can lead to breakpoints occurring at normalised
137 primary driver strengths 0.312 (reduction from baseline: 0.036 [10.3%]; Figure S2-4D), and the
138 addition of an extra tertiary driver with normalised strength 0.3 can lead to breakpoints at normalised
139 primary strengths 0.270 (reduction from baseline: 0.078 [22.4%]; Figure S2-4D). With all additional
140 drivers, 12.3% of breakpoints observed in the Lake phosphorus model occurred at primary driver
141 strengths below the minimum threshold required to result in a breakpoint when the primary driver is
142 acting in isolation (Lake Chilika: 1.2%; Easter Island: 14.8%; TRIFFID: 7.7%; Table S2-1).

143

144 Next, for each of the four models, the trajectories of the primary slow drivers were randomly
145 perturbed by the addition of noise (Methods Section 2.3). Noise was generated within the system
146 dynamics software used to run the models (STELLA³⁹) by randomly sampling per timestep from a
147 normal distribution with a mean value of 0 and standard deviation of σ (sigma), meaning that random
148 perturbations on the system could work in both positive ($\sigma > 0$) and negative directions ($\sigma < 0$). The
149 value of σ was randomly sampled once per simulation to explore the effects of different noise scales
150 on the time to reach the breakpoint date (Methods Section 2.3). The addition of high noise
151 (normalised σ values > 0.666) shows that increasing the variability of the primary slow driver (in
152 isolation) across all four models can bring forward the date of system collapse (Figure 3).

153

154 The effects outlined above are synergistic – combining multiple drivers with noise further reduces the
155 breakpoint date beyond the effects of either multiple drivers or noise acting alone (Figure 4). For
156 example, at a normalised slow baseline driver strength of 0.3 in the Easter Island model (Figure 4B),
157 the addition of low uncoupled noise (normalised σ values ≤ 0.333) with all possible additional drivers
158 switched on with normalised strengths of over 0.666 (i.e. ‘high’ secondary and tertiary trajectories)
159 brings the median breakpoint forward from timestep 1179 to timestep 426 (63.8% reduction),
160 whereas high noise levels (defined as normalised σ values > 0.666) brings the breakpoint forward from
161 timestep 1179 to timestep 225 (80.9% reduction). The finding that the breakpoint date is most
162 advanced by the combination of high noise and high secondary trajectories is consistent across the
163 other three models, with the median breakpoint date at a normalised slow baseline driver strength of
164 0.3 changing from year 2047 to year 2035 (37.5% reduction) for Lake Chilika, timestep 238 to timestep
165 92 (61.3% reduction) for TRIFFID, and timestep 848 to timestep 388 (54.2% reduction) for Lake
166 phosphorus. Across all combinations of noise and multiple drivers, 1.7%, 7.5%, 6.6% and 8.9% of
167 modelled breakpoints occurred at primary driver strengths below the minimum threshold required to
168 result in a breakpoint when acting in isolation for Lake Chilika, Easter Island, TRIFFID and Lake
169 phosphorus respectively (Table S2-4).

170

171 All results presented above are robust to different modelling and monitoring decisions. For example,
172 these results are consistent regardless of whether the noise is coupled to (i.e. allowed to grow with)
173 the magnitude of the primary slow driver or uncoupled and sampled from a constant distribution
174 (Figure S2-2 & S2-3; Table S2-3 to S2-5), and irrespective of whether linear, non-linear or threshold-
175 type boundaries⁴⁰ are used to define the breakpoints (SI-4; Figures S4-1 to S4-6).

176

177 Discussion

178 Previous findings have supported the idea that Earth’s subsystems may interact to the extent that an
179 abrupt shift in one raises the probability that a shift may occur in another^{41–43}. In this paper we
180 have explored through four ecosystem models how these interactions may alter the timing of ATDCs
181 through the effects of strengthened drivers, multiple drivers and higher internal variability or
182 noise. The potential effects are substantial with combinations of a strengthened main driver, an
183 additional driver and noise giving at least 38-81% reductions in the future date of a predicted ATDC
184 compared to estimates for a non-interacting system with a constant single driver and no
185 noise. Importantly, the effect per unit time on bringing forward an ATDC is greatest at low driver
186 trajectories, which further strengthens the suggestion that abrupt Earth system changes may occur
187 sooner than we think (SI-1). Our findings also show that 1.2-14.8% of ATDCs can be triggered by
188 additional drivers and/or noise below the threshold of driver strengths required to collapse the system
189 if only a single driver were in effect.

190

191 Overall, we find that as the strength of a main driver increases, the systems collapse sooner. Adding
192 multiple drivers brings collapses further forward, as does adding noise, and the two effects can be
193 synergistic. However, the relative importance of these changes varies across systems. For the Chilika
194 fishery, the most influential driver is captured as the primary driver and so additional drivers have
195 limited influence, with the addition of noise in the primary driver bringing the breakpoint date much
196 closer to the present. For Easter Island, TRIFFID, and Lake phosphorus, the opposite is true – the
197 addition of high levels of noise in the primary driver advances the date of system collapse far less than
198 additional drivers. Thus, while the earliest collapses in all the systems are found when both additional
199 drivers and noise are applied, an important implication for real world governance is that the precise
200 importance of individual driver trajectories and noise is system-dependent.

201

202 Earlier occurrence of abrupt threshold-dependent changes

203 Our results show that systems do not collapse at a constant level of cumulative stress (i.e., total stress
204 built up over time) irrespective of the rate of stress change (SI-5) but rather underline the importance
205 of rate over accumulated stress^{18–20}. Simulations where the primary, secondary or tertiary drivers

206 change more rapidly tend to shift earlier and are less able to absorb cumulative stress (Figure SI5-1).
207 Thus, the same ecosystem can collapse as a result of sustained/cumulative pressure of a slower driver,
208 but will likely collapse faster if the rate of change is increased^{18–20}. Increasingly fast driver rates will
209 eventually overwhelm the ability of balancing feedback loops to compensate for increased stress on
210 the system; thus, signifying a loss of resilience. In the absence of strong balancing loops, a fast driver
211 allows reinforcing feedback loops to grow (SI-6). The driver may also re-energise dormant reinforcing
212 feedback loops or allow new coupled, reinforcing feedback mechanisms to emerge (cf. ⁴⁴). For the
213 Easter Island, TRIFFID and Lake phosphorus models, as the balance of feedback loops shifts towards
214 reinforcing loops, the probability that the system will be driven out of its attractor into an ATDC
215 increases (SI-6). Additional drivers limit further the balancing ability of balancing feedback loops and
216 increase the probability of collapse. For Lake Chilika, the pre-ATDC phase is dominated by reinforcing
217 feedback loops driving fisher population growth towards dangerous levels, with collapse coinciding
218 with the growth of balancing feedbacks in the form of reduced fish populations. These rebalance the
219 system by limiting the effectiveness of the fisher population's fishing efforts (Figure S6-1).

220

221 In our analysis, the rise in driver stress is continuous over time. Where the stress is applied in discrete
222 events, for example, wildfire events, the same response can be expected where elapsed time between
223 events is insufficient for balancing feedback loops to rebalance the system or where significantly large
224 stress events motivate additional amplifying loops. This is similar to the impact of extreme events (i.e.,
225 noise, Figures 3 and 4), which has the ability to push a system out of its attractor temporarily or
226 permanently; an effect that strengthens as the system becomes increasingly sensitive to perturbations
227 close to a potential ATDCs^{19,23}. However, sequences of extreme events from multiple drivers, such as
228 extreme drought followed by extreme rainfall, may only act antagonistically where sufficient time
229 allows for the system to repair the extreme impacts. Our study only looks at driver noise; there could
230 coincidentally or equally be natural 'state' change/noise (vertical axis on phase-plot figures) – for
231 example, natural tree mortality, natural lake infilling, fluctuating populations in ecosystems, or ageing
232 population, behavioural/psychological changes in the social domain – all of which could alter the
233 probability of ATDCs even in the absence of, or changes in, the external drivers^{19,23}.

234

235 Moving forward

236 These results have research implications for further developing and applying models of ecosystems to
237 study ATDCs. Whilst our findings derive from models based on real-world systems, the greater
238 complexity of reality may limit the transferability of our results. The Lake Chilika model is the most
239 complex of the four models, with upwards of 100 model variables capturing hydroclimatic,
240 ecohydrological, fishery and socio-economic dynamics interacting to create four balancing loops and
241 seven reinforcing loops – and is validated against historical data³³. Of all the models, it shows the least
242 dramatic reductions in the date of any ATDC (SI-1). Therefore, it is plausible that more complex
243 systems will have stronger regulating mechanisms that stabilise the system through sets of balancing
244 feedback loops⁴⁴, constraining the more extreme of our findings.

245

246 Mechanistically, in simpler models, such as the Lake phosphorus model, regime shifts may be
247 triggered by a single feedback loop. In more complex models (and likely ecosystems), our analysis of
248 feedbacks strengths shows evidence for an instability cascade through the system via multiple
249 feedback loops. For example, the collapse in the Easter Island human population reflects the
250 cumulative effects of several feedback loops triggered by over-harvesting the tree population.
251 Growing instability weakens the balancing feedbacks for the tree population, rat population and
252 agricultural carrying capacity (Figure S6-2), allowing the reinforcing loop for the decline in human
253 population to strengthen. In general, increasing driver strengths can trigger these mechanisms earlier,
254 whereas additional drivers have the ability to shift the nature of the cascade (e.g. including/excluding
255 different feedbacks; Figures S6-5 to S6-8). However, in spatial terms, multiple interacting feedback
256 mechanisms may lead to spatial re-organisation which slows the rate of collapse^{45,46}, with stochasticity

257 promoting temporal stability – particularly in local regions with small populations²⁴. There is the
258 possibility, too, that interconnections could have weakening effects and, where the impacts are slower
259 than the system response, extreme events could counteract each other. Thus, our quantitative
260 findings could be viewed as representing worst-case scenarios for the different ecosystems⁷.

261

262 Nevertheless, the finding that additional stress produces qualitatively similar emergent phenomena
263 in a range of simulation models should not be dismissed lightly^{47,48}. The consistency across models
264 representing varying processes, interactions and contexts may indicate that equifinality makes the
265 accurate representation of internal system dynamics less important than the external drivers/stresses
266 in simulating complex realities⁴⁹. Clearly, model development is required to better capture the
267 diversity of system elements, interactions, and feedbacks for more complex systems, and in particular,
268 more realistic coupling of human decision making and ecological/environmental dynamics. With the
269 exception of Lake Chilika³³, each model in this study was originally created to study the impact of a
270 primary driver influenced by predominantly external anthropogenic processes, presumably the driver
271 perceived as the most impactful. Our results show that this assumption may not be the case (e.g.
272 Easter Island) and models should include a range of plausible drivers and scenario combinations if they
273 are to avoid underestimating the risk of ATDCs. Moreover, new ecosystem models should allow for
274 the growth of feedback loops and long-term simulations in order to observe the mechanisms that
275 underpin ATDCs^{48,50}. For example, more realistic social-ecological coupling may lead to shifts in the
276 human decisions capable of either shifting an ATDC much closer to the present or avoiding it
277 completely. Monitoring of real-world systems should therefore capture multiple plausible drivers,
278 their variability, and their feedbacks to social systems. More ATDCs will occur unexpectedly if the focus
279 on perceived main drivers ignores other drivers that increase cumulative stress and gradually reduce
280 the resilience of systems, as exemplified in the lake water regime shift at Erhai, western China²⁸. There,
281 abrupt lake eutrophication was initially perceived to have been driven by transgression of a threshold
282 in nutrient enrichment driven by agricultural runoff, but historical analysis has shown that the shift
283 was also affected by lake water level management, seasonal climate and fish farming⁴⁴.

284

285 Significant research has focused on identifying early warning metrics linked to critical slowing down
286 theory which applies primarily to ‘equilibrium’ system states with single, slow drivers⁵¹. If, as we
287 indicate, real world tipping elements are more likely to be driven by multiple, fast drivers and extreme
288 events, it is less likely that early warning signals in the frequency domain will be observed^{20,51} for noise-
289 induced thresholds. Certainly, excluding noise from model systems, whilst a potentially useful
290 simplification for theoretical understanding, risks creating a false sense of security by overestimating
291 the distance remaining before critical thresholds are breached in the real world where multiple drivers
292 and noise are abundant^{27,52}. Therefore, alternative approaches to identifying resilience loss in real
293 systems prior to ATDCs through structural metrics^{53–55} and early warning signals generated by agent-
294 based models⁵⁰ should be considered more widely.

295

296 Previous studies of interactions between tipping elements have focused on large scale systems and
297 suggest significant social and economic costs from the second half of the 21st century onwards^{42,56}.
298 Our findings suggest the potential for these costs to occur sooner. For example, it is not clear whether
299 the IPCC’s estimate for a tipping point in the Amazon forest prior to 2100¹¹ includes the possibility for
300 interacting drivers and/or noise; if not, our findings suggest a breakdown may occur several decades
301 earlier (SI-1). This would occur where local scale failures in elements (such as species populations, fish
302 stocks, crop yields and water resources) combine with more extreme events (such as wildfires and
303 droughts) to precondition the large-scale system, already vulnerable to the influence of other large-
304 scale tipping elements, to collapse earlier – a meeting of top-down and bottom-up forces (SI-1). This
305 vertical integration of forces is reinforced by the rising trend in global warming that already represents
306 a spatial integrator which may be expected to strengthen before it subsides. Clearly, climate
307 economics need to incorporate these synergistic and cumulative effects that are occurring at local and

308 regional scales into larger scale models where they are currently lacking^{57,58}. The dominance of
309 accelerating trends in global time-series of economic consumption [e.g.^{9,59}] makes our finding that
310 ramping up the main driver is the easiest way to bring forward an ATDC particularly worrying. Similarly,
311 the implication for regions experiencing more extreme events is that an ATDC may occur even before
312 the main driver has ramped up.

313

314 The commonality of findings across four well-studied ecosystems has potentially profound
315 implications for our perception of future risks associated with the climate and ecological crises. While
316 it is not currently possible to predict how climate-induced ATDCs and the effects of local human
317 actions on ecosystems connect across temporal and spatial scales, our findings show the potential for
318 each to reinforce the other. The ability of present policy and practice to prevent an ever-deepening
319 vortex of degradation in local and regional ecosystems requires urgent investigation⁷.

320

321 **Methods**

322

323 1. Overview of systems models

324 Here we briefly describe the four previously published models used to investigate the effects of
325 multiple drivers and noise upon the timing of ATDCs. Each model was replicated and simulated within
326 the system dynamics software STELLA Architect v.1.6.1³⁹, with outputs exported into CSV files as time
327 series and analysed in the statistical software R v.4.1.0⁶⁰. The models, example data and code used in
328 the analyses are available via: <https://doi.org/10.5281/zenodo.7946433>.

329

330 The **Lake Chilika fishery** model^{21,33} is a social-ecological model designed to simulate the future fish
331 population and catch trajectories of the Chilika lagoon, Odisha, India. The model is able to explore the
332 impacts of multiple slower drivers (i.e., fisher population growth and increased rainfall and
333 temperatures under climate change) and multiple faster drivers (i.e. abrupt changes in fish prices and
334 fishing gear) on the sustainability and resilience of the fish population until 2100. As described in detail
335 in ³³, the model includes coupling between multiple social and ecological components of the system.
336 First, the efficiency of fish catch efforts is proportional to the fish population density within the lagoon
337 (i.e. as fish density declines, catch per unit effort also decreases). Second, as a form of environmental
338 carrying capacity, the fisher population growth is proportional to the total number of livelihoods
339 supportable by the overall fishery value, which is derived from the total fish catch in any given month.
340 Third, fishers may invest their fishing revenues into more intensive fishing gear (i.e. motorboats),
341 which also has implications for fish catch and fish stock health over time. The model is also able to
342 simulate multiple natural resource governance approaches (e.g. fishing quotas and alternative
343 livelihoods), although the model runs conducted here are all under the baseline governance scenario³³
344 (i.e. the tidal outlet between the lagoon and the Bay of Bengal is reopened every ten years to
345 rejuvenate fish migration and lagoon salinity). The model has been previously validated against
346 empirical data through standard behaviour matching techniques and Monte Carlo sensitivity
347 analysis³³. The Lake Chilika model is run for a total of 1536 timesteps (months), with each timeseries
348 aggregated to the annual scale (c.1973-2100). Future trajectories, detailed in Method Sections 2.2-
349 2.4, activate from timestep 504 (i.e. January 2015) after the completion of the historical
350 parameterisation and validation periods³³.

351

352 The **Easter Island** model aims to explore alternative hypotheses behind the collapse of the Easter
353 Island civilisation³⁶. The initial parameterisation of the model here is the same as the 'ecocide'
354 configuration detailed in ³⁶. The main internal social-ecological feedback driving model dynamics is
355 the balancing feedback between human population growth, tree coverage and land clearance,
356 whereby the overharvesting of the primary resource (palm forest) can lead to overshoot dynamics
357 and the eventual demise of the human population (i.e. 'ecocide'). As noted in ³⁶ (p.1): "*While it is*
358 *obvious that the islanders were not directly living from palm trees, the forest provided several valuable*

359 and difficult to substitute ecological services, including food from fruits and palm nuts, timber to
 360 construct houses and sea-going canoes for fishing". In addition to this main internal social-ecological
 361 feedback, multiple external variables can be modified to change the speed of human population
 362 growth, including the tree clearance rate per capita, the maximum carrying capacity of the agricultural
 363 system (i.e. to help support human population growth), and the mortality rate of trees (i.e.
 364 representative of potential disease outbreaks). The model is run for 1500 timesteps (years), with
 365 future scenarios active from the first timestep (Method Sections 2.2-2.4).

366
 367 The **TRIFFID** model is a modified version of The Hadley Centre Dynamic Global Vegetation Model,
 368 originally developed by Cox *et al.*³⁸ to explore the effects of atmospheric CO₂ concentrations on the
 369 rate of Amazon dieback. Here we simulate the modified version developed by Ritchie *et al.*²⁷, which is
 370 based around a central Lotka-Volterra equation describing the change in vegetation coverage as the
 371 primary external driver (local atmospheric temperatures) increases. On any given timestep, the
 372 change in vegetation coverage (dv/dt) is driven by a temperature dependent growth term and an
 373 externally set disturbance rate:

$$374 \quad \frac{dv}{dt} = gv(1 - v) - yv \quad (\text{Equation 1a})$$

$$375 \quad g = g_0 \left[1 - \left(\frac{T_i - T_{opt}}{\beta} \right)^2 \right] \quad (\text{Equation 1b})$$

$$376 \quad T_l = T_f + (1 - v)\alpha \quad (\text{Equation 1c})$$

377 Where v is the vegetation coverage, T_f is the temperature forcing parameter (Methods Section 2.3), g
 378 is the vegetation growth rate, g_0 is the maximum growth rate (2/year), y is the disturbance rate
 379 (Methods Section 2.4), T_l is the local temperature, T_{opt} is the optimal temperature (28°C), β is the half-
 380 width of the growth versus temperature curve (10°C) and α is the difference in temperature between
 381 surface bare soil and forest (5°C). Therefore, the growth term is assumed to be parabolic with the local
 382 temperature (Equation 1b), meaning that once the local temperature increases beyond the optimal
 383 temperature, negative tree growth ensues [i.e. additional tree mortality²⁷], which in turn leads to an
 384 increase in temperature (Equation 1c), which may eventually produce the runaway loss in tree
 385 coverage. Although the meaning of the disturbance rate is not specified by Ritchie *et al.*²⁷, it may proxy
 386 human-induced ecosystem stresses such as deforestation for agricultural land and disease-driven
 387 forest dieback. The model is run for 500 timesteps, with future trajectories active from the first
 388 timestep (Method Sections 2.2-2.4).

389
 390 The **Lake phosphorus** model is a simplified version of the original 'lake response to P input and
 391 recycling' model³⁷, as modified by Wang *et al.*²⁸. The model is designed as a simple ecosystem model,
 392 with lake water phosphorus concentration driven by a generic external phosphorus input (which may,
 393 for example, proxy external inputs from agricultural runoff, sewage, and industrial discharges from
 394 factories, construction sites, and urban areas)⁶¹. In turn, lake water phosphorus is recycled back into
 395 the system as an ecological reinforcing feedback loop, proportional to the lake phosphorus
 396 concentration on any given timestep. Phosphorus is also removed from lake waters via sedimentation,
 397 where the volume removed in sediment is proportional to the phosphorus concentration of the lake.
 398 Therefore, on any given timestep, the change in lake phosphorus concentration (dP/dt) equals:

$$399 \quad dP = \left[a - sP + r \frac{P^n}{P^n + 1^n} \right] dt \quad (\text{Equation 2})$$

400 Where P is phosphorus concentration, a is phosphorus input rate (Methods Section 2.3), r is the
 401 maximum recycling rate (Methods Section 2.4), s is the phosphorus loss rate (Methods Section 2.4), n
 402 is the strength of the recycling response to phosphorus concentrations ($n = 8$) and t is time. The model
 403 is run for 1000 timesteps (unitless), with future scenarios active from the first timestep (Method
 404 Sections 2.2-2.4). Given the simplicity of this model, an area for future research could be expanding
 405 the original model to explore how adaptive management mechanisms may help to avoid ecosystem
 406 thresholds, for example, by linking government fertiliser incentives to lake phosphorus levels as the
 407 ecosystem approaches a threshold.

408

409 2. Generation of future scenarios

410 Using the above models, we performed four *in silico* experiments (presented visually in Figure 1):

- 411 - **Experiment #1:** only the primary slow driver in each model changes over time, and all other
- 412 drivers remain constant (Figure 2 baseline);
- 413 - **Experiment #2:** multiple slow rates, with up to two additional (i.e., 'secondary' and 'tertiary')
- 414 slow trajectories on top of the primary driver changing over time (Figure 2 multiple drivers);
- 415 - **Experiment #3:** the addition of noise to the primary trajectory (Figure 3), with all other drivers
- 416 held constant. The magnitude of noise may be either coupled or uncoupled from the
- 417 trajectory of the primary driver (Methods Section 2.3);
- 418 - **Experiment #4:** the addition of noise to the primary driver, with up to two additional slow
- 419 drivers (Figure 4). The magnitude of noise may be either coupled or uncoupled from the
- 420 trajectory of the primary driver (Methods Section 2.3).

421 In order to survey a wide range of future trajectories (Methods Sections 2.2) and generate a sufficient

422 number of simulations that collapsed (Methods Section 3), each of the models were ran for the

423 following number of iterations (including both 'coupled' and 'uncoupled' settings):

- 424 - Chilika fishery: 70,000
- 425 - Easter Island: 70,000
- 426 - TRIFFID: 70,000
- 427 - Lake phosphorus: 120,000

428 In turn, to maximise computational efficiency both in STELLA and in R, the following logic was applied

429 to the in-built Monte Carlo function in STELLA to automatically generate the four different experiment

430 types described above (the baseline primary driver always remains 'on/active'):

- 431 - IF $\mu_1 > 0.4$ THEN *Secondary driver active* ELSE *Secondary driver remains at default value*
- 432 - IF $\mu_2 > 0.4$ THEN *Tertiary driver active* ELSE *Tertiary driver remains at default value*
- 433 - IF $\mu_3 > 0.4$ THEN *Noise active* ELSE *Noise level remains at zero*

434 Where μ_1, μ_2 and μ_3 represent 'on switches', with values randomly sampled from uniform distributions

435 between 0 and 1 per simulation. The number of simulations per model experiment which showed

436 ATDCs are detailed in Table S3-1.

437

438 Whilst some insights could be obtained deterministically⁶², this is not possible for all models (e.g. Lake

439 Chilika) nor for all experiments (i.e. those involving additional noise). Thus, undertaking these model

440 runs and analyses of the outputs (below) is the most consistent, feasible approach suitable across all

441 models and experiments, allowing for comparisons across experiments, as well as investigation of

442 synergistic impacts – fulfilling our primary aim of investigating the impact of the interaction of fast

443 drivers, multiple drivers and system noise on the timing of tipping points in ecosystems.

444

445 In order to investigate Experiment #1, each of the four models has one primary baseline driver which

446 changes from its default value in every simulation:

- 447 - Lake Chilika fishery: Fisher population growth rate (net difference between the birth rate per
- 448 1000 population and the death rate per 1000 population)
- 449 - Easter Island: Tree clearance rate (trees/person/year)
- 450 - TRIFFID: local temperature (°C)
- 451 - Lake phosphorus: Phosphorus input rate (unitless)

452 Baseline outputs were generated with the Primary driver active AND the Secondary and Tertiary driver

453 remaining at its default value AND the Noise level remaining at zero (Table S3-2). In turn, the Monte

454 Carlo sensitivity analysis function in STELLA randomly samples a future change trajectory for the

455 primary slow driver per simulation (as plotted on the horizontal axes of Figures 2-4). The primary

456 trajectory is sampled between the lower and upper limits of uniform distribution bounds, meaning

457 that there is a uniform likelihood of selecting any given trajectory between the bounds (Table S3-2).

458 A future change trajectory of '0' would cause no change from the default value; the maximum

459 trajectory change limits for each of the models can be seen in Table S3-2.

460

461 The built-in STELLA 'TIME' function generates future scenario trajectories that change linearly over
462 time (i.e., with a constant gradient over the model horizon). Therefore, the value of the primary driver
463 at any given timestep equals:

$$464 \quad \text{Scenario value}_{i,t} = \text{TIME}_{i,t} \times \left(\frac{\text{Maximum trajectory value}_i}{\text{Total number of timestep in model}} \right)$$

465 (Equation 3)

466 Where 'i' equals the simulation number and 't' equals the timestep (e.g. t = 1, 2, 3... total number of
467 timesteps in model). Using the Easter Island model as an example: if a maximum tree clearance value
468 of 7 has been sampled for the given simulation, then its value after 500 timesteps would be equal to
469 500 x (7/1500) = 2.333. The plausible trajectory funnels for each of the primary drivers are plotted in
470 Figure S3-1.

471

472 To simulate Experiment #2, 'secondary' and 'tertiary' driver trajectories are also activated using the
473 following logic:

- 474 - 'Secondary': Primary driver active AND Secondary driver active AND Tertiary driver remains
475 at default value AND Noise level remains at zero OR
- 476 - 'Tertiary': Primary driver active AND Secondary driver remains at default value AND Tertiary
477 driver active AND Noise level remains at zero OR
- 478 - 'All': Primary driver active AND Secondary driver active AND Tertiary driver active AND Noise
479 level remains at zero

480 For each model, this specifically involved the following variables (Table S3-2):

- 481 - Lake Chilika fishery: (i) Annual rainfall totals and mean near-surface air temperatures, as per
482 IPCC (2013) climate change projections for the east coast of India (ii) Price of fish per unit (i.e.
483 Indian rupee/kg), leading to a more commercially-oriented fishery, with an increasing number
484 of fishers able to upgrade from traditional fishing boats to more intensive motorboats³³.
- 485 - Easter Island: (i) Agricultural carrying capacity of the system, which enables a higher human
486 population to be supported per unit of land cleared for agriculture; (ii) The mortality rate of
487 trees as a proxy for a disease-spread event.
- 488 - TRIFFID: (i) Temperature-independent disturbance rate of vegetation coverage, i.e., causes of
489 forest clearance which are not directly linked to temperature changes (e.g. deforestation).
490 Note: Due to the small size of the model, TRIFFID does not have a tertiary driver.
- 491 - Lake Phosphorus: (i) Rate of phosphorus recycling within the lake environment, (ii) Rate of
492 phosphorus removal from the lake via sedimentation.

493 For the Lake Chilika and Easter Island models, these additional drivers are external forcings (similar to
494 the primary driver). However, since the TRIFFID and Lake phosphorus models are designed with only
495 a single external forcing, additional drivers were also generated internally by altering parameters that
496 operate on state variables. Whilst mathematically, internal and external forcings are fundamentally
497 different things, both potentially impact the state of the system and, ecologically, changing internal
498 model parameters can act as a proxy for an external process causing that change. For example, in the
499 Lake phosphorus model we have a system with a bifurcation in one dimension of slow external forcing
500 (α) and we additionally vary internal parameters of the system (P recycling rate and P removal rate)
501 as a proxy for, for example, anthropogenic disturbance impacting the species composition within the
502 lake⁶³.

503

504 Each of the additional driver trajectories are produced via the same approach as in Equation 3: the
505 Monte Carlo sensitivity analysis function in STELLA randomly samples a trajectory between the lower
506 and upper bounds of a uniform distribution for each driver (Table S3-2); in turn, the TIME function
507 linearly increases the value of the driver from its default value to its sampled trajectory value by the
508 final timestep of the model horizon.

509

510 In order to produce one secondary trajectory per simulation in the Lake Chilika model, the sampling
511 of rainfall and temperature trajectories are connected along a linear gradient, ranging from no change

512 to a combination of +30% rainfall change and +4.5°C temperature change by 2081-2100 relative to
 513 1986-2005 [as per RCP8.5 projections for the east coast of India⁶⁴]. In STELLA, this is operationalised
 514 by the model variable ‘climate change trend’, with Monte Carlo sensitivity analysis in STELLA randomly
 515 sampling a value between 0 and 1 per simulation. As an illustration, if a value of 0.6 was to be sampled,
 516 then the change in rainfall by 2081-2100 (relative to 1986-2005) would equal 0.6*30(%) = 18%, whilst
 517 the change in temperature would equal 0.6*4.5(°C) = 2.7°C.

518

519 In order to investigate Experiment #3 and Experiment #4, the value of each primary slow driver is
 520 perturbed per timestep by randomly generated noise. We simulate a standard Wiener process to
 521 generate noise, equal to $\sqrt{dt} \times N(0,1)$, where ‘dt’ equals change in time and ‘N(0,1)’ is a normal
 522 distribution with a mean of 0 and standard deviation of one. In turn, the product of the Wiener process
 523 is multiplied by the scaling factor ‘sigma’ (σ), providing an overall level of noise to be added to the
 524 value of the primary driver on any given timestep. As per the future trajectories, the magnitude of ‘ σ ’
 525 is randomly sampled once per simulation from uniform distributions, with lower and upper limits
 526 shown in Table S3-2.

527

528 Therefore, building on Equation 3 above, the value of a primary driver at any point in time in
 529 Experiment #3 and Experiment #4 equal:

$$530 \quad \text{Scenario value}_{i,t} = \text{TIME}_{i,t} \times \left(\frac{\text{Maximum trajectory value}_i}{\text{Total number of timestep in model}} \right) + (\sigma_i \times \sqrt{dt} \times N(0,1)_t)$$

531 (Equation 4)

532 Equation 4 as detailed above only refers to the ‘uncoupled’ noise simulations. Therefore, to explore
 533 the effects of ‘coupled’ noise, whereby the magnitude of noise increases with the growth in the
 534 primary driver, 20,000 simulations were run per model spread evenly between Experiments #3 and
 535 #4, with the magnitude of noise coupled to the magnitude of the primary driver trajectory. Given the
 536 differences in the shape of the noise spectrums, we do not directly compare outcomes from the
 537 uncoupled and coupled noise simulations in this study. Instead, the purpose of modelling coupled
 538 noise is to ascertain whether worsening magnitudes of extreme events over time are associated with
 539 earlier ATDCs. In the coupled simulations, Equation 4 is modified to:

$$540 \quad \text{Scenario value}_{i,t} \\ 541 \quad = \text{TIME}_{i,t} \times \left(\frac{\text{Maximum trajectory value}_i}{\text{Total number of timestep in model}} \right) \\ 542 \quad + (\sigma_i \times \sqrt{dt} \times N(0,1)_t \times \text{Change in Scenario value from default}_{i,t})$$

543 (Equation 5)

544 For Experiment #3 (single slow driver plus noise), the runs were generated in STELLA³⁹ with the
 545 following logic: Primary driver active AND Secondary driver remains at default value AND Tertiary
 546 driver remains at default value AND Noise active. For experiment 4 (noise plus multiple slow
 547 drivers), the logic used included:

- 549 - Primary driver active AND Secondary driver active AND Tertiary driver remains at default
 550 value AND Noise active
- 551 - Primary driver active AND Secondary driver remains at default value AND Tertiary driver
 552 active AND Noise active
- 553 - Primary driver active AND Secondary driver active AND Tertiary driver active AND Noise
 554 active

555

556 3. Timeseries breakpoint detection

557 The identification of the timing of the ATDCs in the model runs was a two-step process.

558

559 First, to ensure that we were only analysing model runs that had transitioned (i.e. collapsed) to
 560 quantitatively and qualitatively functionally different states (e.g. fishery collapse, civilisation collapse,

561 forest dieback or lake eutrophication), we assessed whether model outcomes had crossed a pre-
562 defined threshold at any point over the model horizon. For the three models which observe collapses
563 in the outcome variable (i.e. Lake Chilika fishery, Easter Island and TRIFFID), model runs were
564 considered to have reached a collapsed state if the outcome variable reached a value beneath 20% of
565 its initial value at any point during the simulation. This demarcation is therefore representative of
566 Type-1 boundaries defined by Dearing *et al.*⁴⁰, with the numerical value of the boundary in line with
567 the concept that fish stocks may be considered collapsed once their biomass falls beneath 20% of the
568 biomass needed to maintain maximum sustainable yield^{65,66}. In the case of the Lake Chilika fishery
569 model, which has inbuilt social-ecological feedbacks that may trigger the recovery and later re-
570 collapse of the fishery^{21,33}, we subset the timeseries to the period prior to the first timestep beneath
571 20% of the initial fish population. As we are only interested in the initial collapse, not sub-setting this
572 time period would risk capturing subsequent collapses and recoveries in the analysis.

573
574 With lake eutrophication caused by an increase in phosphorus concentrations, a linear threshold
575 beyond which we could be confident that the model had entered a qualitatively different state could
576 not be identified. Therefore, as per the approach taken by Drijfhout *et al.*⁶⁷ for identifying abrupt
577 events in global climate models, we adopted a Dearing *et al.*⁴⁰ Type-2 boundary to include only
578 simulations which reached lake phosphorus concentrations greater than four times the standard
579 deviation (SD) of the pre-ATDC time series. Therefore, runs of the Lake phosphorus model which did
580 not exceed this 4xSD threshold were not considered to reach phosphorus concentrations sufficiently
581 outside of the pre-transition envelope of variability, and were therefore excluded from our analysis.

582
583 The second stage of timeseries breakpoint detection used the optimal breakpoint function of the R
584 package 'strucchange' v.1.5-2⁶⁸ to identify ATDC dates in the time series that had successfully met the
585 above qualifications (i.e. reached an alternative state). As described in Cooper *et al.*²¹, the optimal
586 breakpoint function finds the most significant deviation from stability in classical regression models
587 (Figure S3-2), whereby regressions coefficients shift from one regime to another. Therefore, the
588 breakpoint date is taken as the most significant deviation of the outcome variable *en route* to its
589 qualitatively and quantitatively alternative state.

590

591 4. Boxplots and output graphs

592 For each of the experiments (i.e. Methods Sections 2.1-2.3), boxplots were generated to visualise the
593 distribution of breakpoint dates for each of the slow driver and noise level combinations (Figures 2-
594 4). To standardise the comparisons between experiments, the normalised magnitude (0 → 1) of the
595 primary trajectories (Table S3-2) for each model was plotted on the horizontal axes. In turn, to
596 visualise how the breakpoint dates change with the addition of secondary or noisy stresses over the
597 range of the primary trajectories, model outcomes that tipped (Methods Sections 3.1-3.2) were subset
598 in the statistical software R between normalised primary trajectory values of 0.25-0.35, 0.45-0.55, and
599 0.65-0.75. From here, boxplots for each of the driver combinations (e.g. 'primary only', 'primary and
600 secondary', etc.) and primary driver subsets (e.g. 0.25-0.35, 0.45-0.55 etc.) were graphed in R using
601 the package 'ggplot' [v.3.3.5⁶⁹].

602

603 **Data Availability Statement**

604 The datasets generated during and/or analysed during the current study are available from the
605 corresponding author on reasonable request, with the models used to create these data available in
606 a DOI-minting repository: <https://doi.org/10.5281/zenodo.7946433>.

607

608 **Code Availability Statement**

609 The code used to analyse the modelled data are deposited in a DOI-minting repository:
610 <https://doi.org/10.5281/zenodo.7946433>.

611

612 **Acknowledgments**

613 SW received funding from NE/W005050/1, NE/T00391X/1, ES/T007877/1, ES/R009279/1,
614 AH/W003813/1, and BB/X010961/1. GSC received funding by the UKRI-GCRF Action Against Stunting
615 Hub (Project ref. MR/S01313X/1).

616

617 **Author Contributions Statement**

618 SW, GSC and JAD conceived and wrote the manuscript. GSC ran and analysed the models. JA provided
619 statistically support and conceptualised the figures. All authors edited and approved the final
620 manuscript.

621

622 **Competing Interests Statement**

623 The authors declare no competing interests.

624

625 **Inclusion and Ethics Statement**

626 This research is global in scope, using models that have been appropriately cited throughout. Roles
627 and responsibilities were agreed amongst collaborators ahead of the research.

628

629 **Figure Legends/Captions (for main text figures)**

630

631 **Figure 1: Schematic overview of the framework developed to explore the influence of slow driver**
632 **trajectories and/or noise on the timing of abrupt threshold-dependent changes (ATDCs):** (A) *the four*
633 *systems models simulated in this study (Methods Section 1); (B) schematic representation of a system*
634 *dynamics model (Lake phosphorus model) with its external slow (blue and green) and noisy (red/orange)*
635 *drivers depicted in colour (Methods Section 2); (C) depiction of the four experiment types (Methods*
636 *Sections 2.1-2.3), ranging from changes in the primary baseline driver only (Experiment #1), changes in*
637 *all slow drivers and noise inputs simultaneously (Experiment #4, where ‘a’ and ‘b’ represent noise profiles*
638 *that are uncoupled or coupled to the primary driver trajectory, respectively): darker colours*
639 *schematically represent steeper trajectories and/or higher noise levels; (D) the two linear techniques*
640 *used to check whether outcomes shift into a functionally different state (Methods Section 3.1) – the top*
641 *panel is applied to Lake Chilika, Easter Island and TRIFFID, where the systems collapse from high*
642 *quantitative outcome states to low quantitative outcome states, and the bottom panel is applied to Lake*
643 *phosphorus (where lake phosphorus concentrations shift from low to high); (E) depiction of the*
644 *timeseries breakpoint date recognition (Methods Section 3.1). The Easter Island icon in (A) is made by*
645 *Roundicons and the remaining three icons are made by Freekpiik, as sourced from www.flaticon.com*
646

647

648 **Figure 2 – The relationship between the breakpoint date and the primary (baseline) slow driver for the**
649 **individual (grey) and multiple (coloured) drivers.** *The normalised primary driver trajectories are*
650 *apportioned into three discrete ranges: ‘low’ – 0.25-0.35, ‘mid’ – 0.45-0.55, and ‘high’ – 0.65-0.75. .*
651 *Subplots: (A) Lake Chilika model, primary slow driver: fisher population growth, secondary driver:*
652 *climate change, tertiary driver: fish price; (B) Easter Island model, primary slow driver = tree clearance,*
653 *secondary driver: agricultural carrying capacity, tertiary driver: tree mortality; (C) TRIFFID model,*
654 *primary slow driver: temperature change, secondary driver: disturbance rate; (D) Lake phosphorus*
655 *model, primary slow driver: phosphorus external input, secondary driver: phosphorus recycling rate,*
656 *tertiary driver: phosphorus sedimentation rate. Model timestep units: Lake Chilika, Easter Island and*
657 *TRIFFID run in years; timesteps in Lake phosphorus are unitless. Boxplots depict the median (50th*
658 *percentile), upper quartile (75th percentile) and lower quartile (25th percentile); individual points*
659 *represent outliers which fall outside 1.5 times the interquartile range from the lower and upper quartiles*
660 *(as depicted by the boxplot whiskers). See Table S3-1 for the number of model simulations underpinning*
661 *each boxplot.*

662

663 **Figure 3 – The relationship between the breakpoint date and the primary slow driver (grey) for varying**
664 **levels of uncoupled noise in the primary slow driver (σ), where normalised σ values ≤ 0.333 signify ‘low**

664 noise' (yellow), normalised σ values > 0.333 and ≤ 0.666 signify 'mid noise' (orange), and normalised σ
665 values > 0.666 signify 'high noise' (red; Methods Section 2.3). The normalised primary driver trajectories
666 are apportioned into three discrete ranges: 'low' – 0.25-0.35, 'mid' – 0.45-0.55, and 'high' – 0.65-0.75.
667 Subplots: (A) Chilika model outputs, primary slow driver = fisher population growth; (B) Easter Island
668 model outputs, primary slow driver = tree clearance; (C) TRIFFID model outputs, primary slow driver =
669 temperature change; (D) Lake phosphorus model outputs, primary slow driver = phosphorus input.
670 Model timestep units and boxplot dimensions are the same as in Figure 2; see Table S3-1 for the number
671 of model simulations underpinning each boxplot.
672

673 **Figure 4 – The relationship between the breakpoint date and the primary slow driver (grey) when weak**
674 **(normalised T values ≤ 0.333) and strong (normalised T values > 0.666) multiple driver trajectories are**
675 **combined with weak (normalised σ values ≤ 0.333) and strong (normalised σ values > 0.666) uncoupled**
676 **noise (T = trajectory, N = noise). The normalised primary driver trajectories are apportioned into three**
677 **discrete ranges: 'low' – 0.25-0.35, 'mid' – 0.45-0.55, and 'high' – 0.65-0.75. . Subplots: (A) the Chilika**
678 **model, primary slow driver = fisher population growth, additional driver: climate change and fish price;**
679 **(B) the Easter Island model, primary slow driver = tree clearance, additional drivers: agricultural carrying**
680 **capacity and tree mortality; (C) the TRIFFID model, primary slow driver = temperature change, additional**
681 **driver: disturbance rate; (D) the Lake phosphorus model, primary slow driver = phosphorus, additional**
682 **drivers: phosphorus recycling rate, phosphorus sedimentation rate. Note, the Lake phosphorus model**
683 **(subplot D) did not produce any outcomes between the 0.65-0.75 primary driver range within the 'high**
684 **trajectory, high noise' scenario; however, the median breakpoint date of the adjacent range (0.55-0.65)**
685 **is 346. Model timestep units and boxplot dimensions are the same as in Figure 2; see Table S3-1 for the**
686 **number of model simulations underpinning each boxplot.**
687

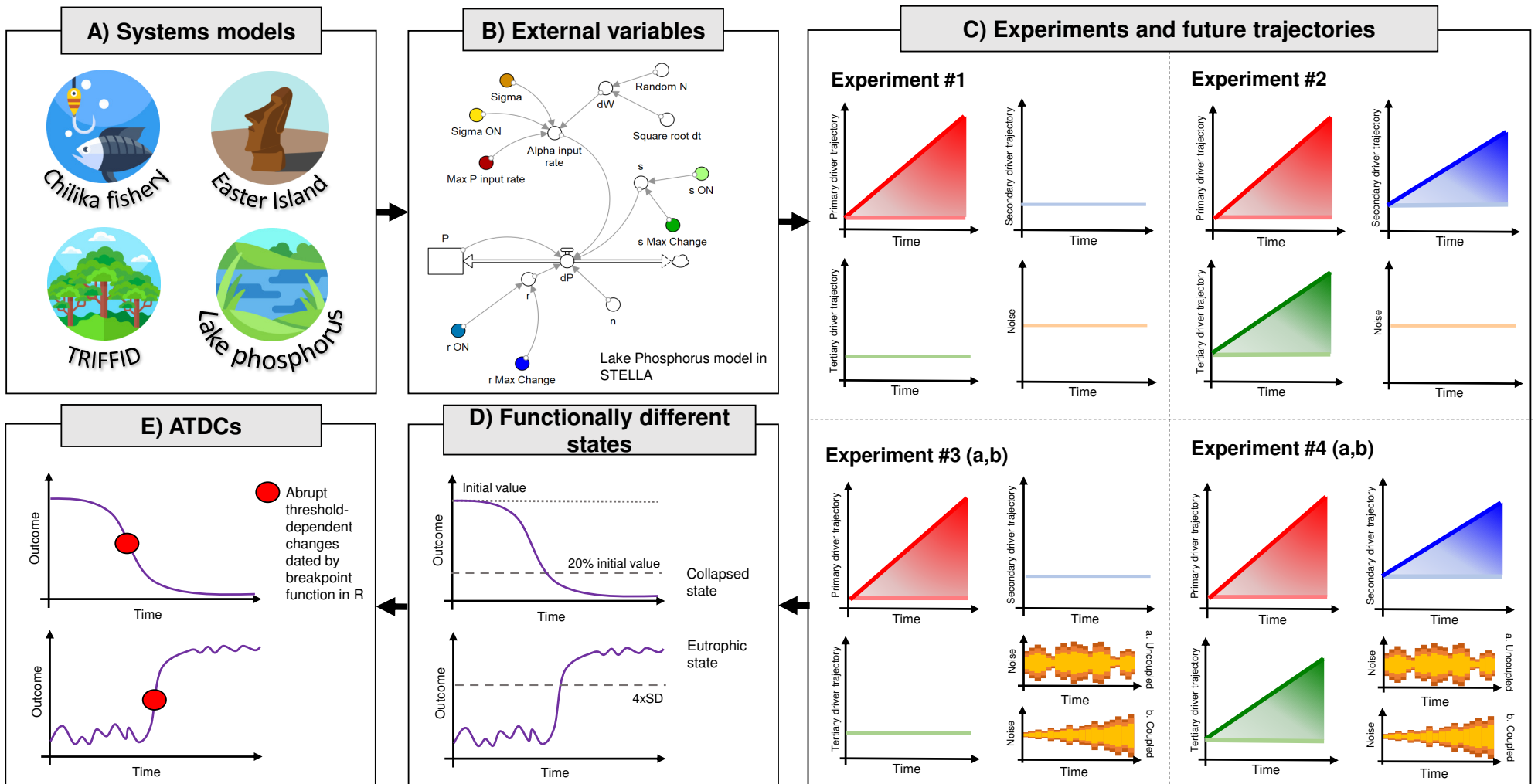
688 References

- 689 1. Beddington, J. *Food, Energy, Water and the Climate: A Perfect Storm of global events.* (2009).
- 690 2. Bradshaw, C. J. A. *et al.* Underestimating the Challenges of Avoiding a Ghastly Future. *Front.*
691 *Conserv. Sci.* **0**, 9 (2021).
- 692 3. Retsa, A., Schelske, O., Wilke, B., Rutherford, G. & de Jong, R. *Biodiversity and Ecosystem*
693 *Services A business case for re/insurance.*
694 [https://www.swissre.com/institute/research/topics-and-risk-dialogues/climate-and-natural-](https://www.swissre.com/institute/research/topics-and-risk-dialogues/climate-and-natural-catastrophe-risk/expertise-publication-biodiversity-and-ecosystems-services)
695 [catastrophe-risk/expertise-publication-biodiversity-and-ecosystems-services](https://www.swissre.com/institute/research/topics-and-risk-dialogues/climate-and-natural-catastrophe-risk/expertise-publication-biodiversity-and-ecosystems-services) (2020).
- 696 4. Reichstein, M., Riede, F. & Frank, D. More floods, fires and cyclones — plan for domino
697 effects on sustainability goals. *Nat.* **2021 5927854 592**, 347–349 (2021).
- 698 5. Scheffer, M. *et al.* Anticipating Critical Transitions. *Science (80-).* **338**, 344–348 (2012).
- 699 6. Kareiva, P. & Carranza, V. Existential risk due to ecosystem collapse: Nature strikes back.
700 *Futures* **102**, 39–50 (2018).
- 701 7. Kemp, L. *et al.* Climate Endgame: Exploring catastrophic climate change scenarios. *Proc. Natl.*
702 *Acad. Sci.* **119**, e2108146119 (2022).
- 703 8. Steffen, W. *et al.* Planetary boundaries: Guiding human development on a changing planet.
704 *Science (80-).* **347**, (2015).
- 705 9. Ripple, W. J., Wolf, C., Newsome, T. M., Barnard, P. & Moomaw, W. R. World Scientists'
706 Warning of a Climate Emergency. *Bioscience* **70**, 8–12 (2020).
- 707 10. Secretariat of the Convention on Biological Diversity. *Global Biodiversity Outlook 5.*
708 www.cbd.int/GBO5 (2020).
- 709 11. IPCC. Summary for Policymakers. in *Climate Change 2021: The Physical Science Basis.*
710 *Contribution of Working Group I to the Sixth Assessment Report of the Intergovernmental*
711 *Panel on Climate Change* (eds. Masson-Delmotte *et al.*) 1–3949 (Cambridge University Press,
712 2021).
- 713 12. Büntgen, U. *et al.* Recent European drought extremes beyond Common Era background
714 variability. *Nat. Geosci.* **2021 144 14**, 190–196 (2021).

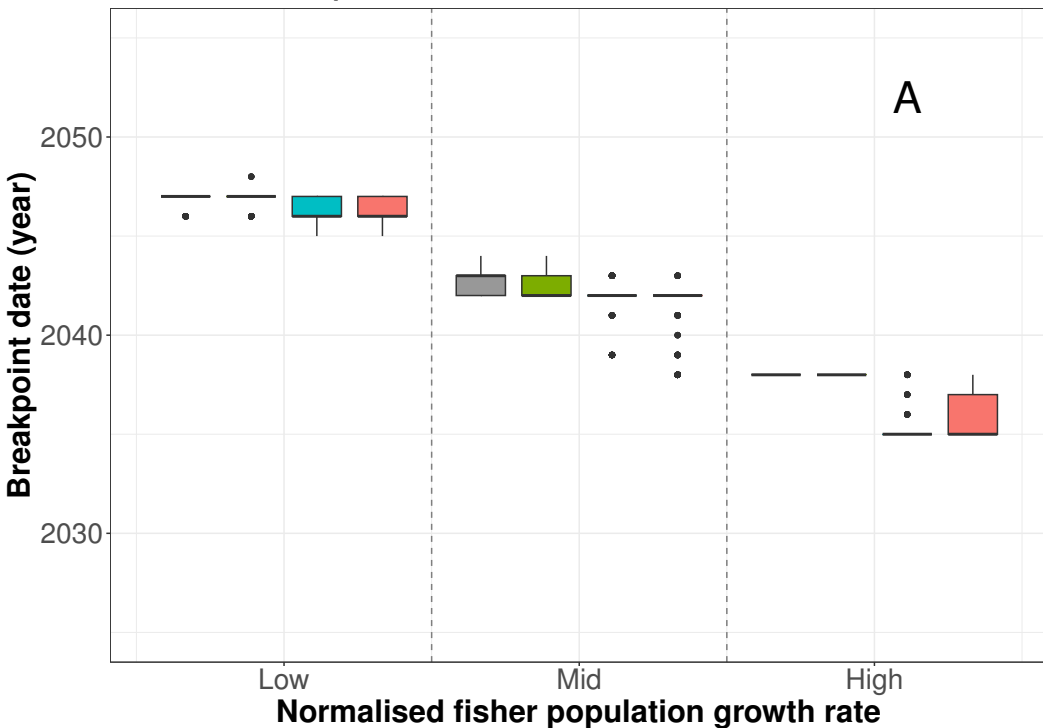
- 715 13. Abram, N. J. *et al.* Connections of climate change and variability to large and extreme forest
716 fires in southeast Australia. *Commun. Earth Environ.* 2021 21 2, 1–17 (2021).
- 717 14. Toreti, A., Cronie, O. & Zampieri, M. Concurrent climate extremes in the key wheat producing
718 regions of the world. *Sci. Reports* 2019 91 9, 1–8 (2019).
- 719 15. Vogel, M. M., Hauser, M. & Seneviratne, S. I. Projected changes in hot, dry and wet extreme
720 events' clusters in CMIP6 multi-model ensemble. *Environ. Res. Lett.* 15, 094021 (2020).
- 721 16. Gaupp, F., Hall, J., Mitchell, D. & Dadson, S. Increasing risks of multiple breadbasket failure
722 under 1.5 and 2 °C global warming. *Agric. Syst.* 175, 34–45 (2019).
- 723 17. McKay, D. I. A. *et al.* Exceeding 1.5°C global warming could trigger multiple climate tipping
724 points. *Science (80-.)*. 377, (2022).
- 725 18. Siteur, K., Eppinga, M. B., Doelman, A., Siero, E. & Rietkerk, M. Ecosystems off track: rate-
726 induced critical transitions in ecological models. *Oikos* 125, 1689–1699 (2016).
- 727 19. Ashwin, P., Wieczorek, S., Vitolo, R. & Cox, P. Tipping points in open systems: bifurcation,
728 noise-induced and rate-dependent examples in the climate system. *Philos. Trans. R. Soc. A*
729 *Math. Phys. Eng. Sci.* 370, 1166–1184 (2012).
- 730 20. O'Keeffe, P. E. & Wieczorek, S. Tipping Phenomena and Points of No Return in Ecosystems:
731 Beyond Classical Bifurcations. *SIAM J. Appl. Dyn. Syst.* 19, 2371–2402 (2019).
- 732 21. Cooper, G. S., Willcock, S. & Dearing, J. A. Regime shifts occur disproportionately faster in
733 larger ecosystems. *Nat. Commun.* 11, (2020).
- 734 22. Arani, B. M. S., Carpenter, S. R., Lahti, L., Van Nes, E. H. & Scheffer, M. Exit time as a measure
735 of ecological resilience. *Science (80-.)*. 372, (2021).
- 736 23. Thompson, J. M. T. & Sieber, J. Predicting Climate Tipping as a noisy bifurcation: A Review.
737 *Int. J. Bifurc. Chaos* 21, 399–423 (2011).
- 738 24. Wilson, W. G. Resolving discrepancies between deterministic population models and
739 individual-based simulations. *Am. Nat.* 151, 116–134 (1998).
- 740 25. Thompson, R. M., Beardall, J., Beringer, J., Grace, M. & Sardina, P. Means and extremes:
741 building variability into community-level climate change experiments. *Ecol. Lett.* 16, 799–806
742 (2013).
- 743 26. Kreyling, J., Jentsch, A. & Beier, C. Beyond realism in climate change experiments: gradient
744 approaches identify thresholds and tipping points. *Ecol. Lett.* 17, 125-e1 (2014).
- 745 27. Ritchie, P. D. L., Clarke, J. J., Cox, P. M. & Huntingford, C. Overshooting tipping point
746 thresholds in a changing climate. *Nat.* 2021 5927855 592, 517–523 (2021).
- 747 28. Wang, R. *et al.* Flickering gives early warning signals of a critical transition to a eutrophic lake
748 state. *Nature* 492, 419–422 (2012).
- 749 29. Groffman, P. M. *et al.* Ecological thresholds: The key to successful environmental
750 management or an important concept with no practical application? *Ecosystems* 9, 1–13
751 (2006).
- 752 30. Renaud, F. G., Birkmann, J., Damm, M. & Gallopín, G. C. Understanding multiple thresholds of
753 coupled social–ecological systems exposed to natural hazards as external shocks. *Nat.*
754 *Hazards* 55, 749–763 (2010).
- 755 31. Kelly, R. A. *et al.* Selecting among five common modelling approaches for integrated
756 environmental assessment and management. *Environ. Model. Softw.* 47, 159–181 (2013).
- 757 32. Filatova, T., Polhill, J. G. & van Ewijk, S. Regime shifts in coupled socio-environmental
758 systems: Review of modelling challenges and approaches. *Environ. Model. Softw.* 75, 333–
759 347 (2016).
- 760 33. Cooper, G. S. & Dearing, J. A. Modelling future safe and just operating spaces in regional
761 social-ecological systems. *Sci. Total Environ.* 651, 2105–2117 (2019).
- 762 34. Tenza, A., Pérez, I., Martínez-Fernández, J. & Giménez, A. Understanding the decline and
763 resilience loss of a long-lived social-ecological system: insights from system dynamics. *Ecol.*
764 *Soc. Publ. online May 02, 2017 | doi10.5751/ES-09176-220215* 22, (2017).
- 765 35. Martin, R. & Schlüter, M. Combining system dynamics and agent-based modeling to analyze

- 766 social-ecological interactions-an example from modeling restoration of a shallow lake. *Front.*
767 *Environ. Sci.* **3**, 66 (2015).
- 768 36. Brandt, G. & Merico, A. The slow demise of Easter Island: Insights from a modeling
769 investigation. *Front. Ecol. Evol.* **3**, 13 (2015).
- 770 37. Carpenter, S. R., Ludwig, D. & Brock, W. A. Management of eutrophication for lakes subject to
771 potentially irreversible change. *Ecol. Appl.* **9**, 751–771 (1999).
- 772 38. Cox, P. M. *et al.* Amazonian forest dieback under climate-carbon cycle projections for the
773 21st century. *Theor. Appl. Climatol.* **2004 781 78**, 137–156 (2004).
- 774 39. ISEE Systems. STELLA Architect: Systems Thinking for Education and Research. at
775 <https://www.iseesystems.com/about.aspx%0A> (2018).
- 776 40. Dearing, J. A. *et al.* Safe and just operating spaces for regional social-ecological systems. *Glob.*
777 *Environ. Chang.* **28**, 227–238 (2014).
- 778 41. Krönke, J. *et al.* Dynamics of tipping cascades on complex networks. *Phys. Rev. E* **101**, 042311
779 (2020).
- 780 42. Kinzig, A. P. *et al.* Resilience and regime shifts: assessing cascading effects. *Ecol. Soc.* **11**, 1–23
781 (2006).
- 782 43. Klose, A. K., Karle, V., Winkelmann, R. & Donges, J. F. Emergence of cascading dynamics in
783 interacting tipping elements of ecology and climate. *R. Soc. Open Sci.* **7**, 200599 (2020).
- 784 44. Wang, R., Dearing, J. A. & Langdon, P. G. Critical transitions in ecosystem state are driven by
785 coupled feedback mechanisms: a case study from Erhai lake, China. *Water* **13**, (2021).
- 786 45. Rietkerk, M. *et al.* Evasion of tipping in complex systems through spatial pattern formation.
787 *Science (80-.).* **374**, (2021).
- 788 46. Bastiaansen, R., Dijkstra, H. A. & Von Der Heydt, A. S. Fragmented tipping in a spatially
789 heterogeneous world. *Environ. Res. Lett.* **17**, 045006 (2022).
- 790 47. Dearing, J. A. *et al.* Navigating the perfect storm: Research strategies for social ecological
791 systems in a rapidly evolving world. *Environ. Manage.* **49**, 767–775 (2011).
- 792 48. Verburg, P. H. *et al.* Methods and approaches to modelling the Anthropocene. *Glob. Environ.*
793 *Chang.* **39**, 328–340 (2016).
- 794 49. Beven, K. A manifesto for the equifinality thesis. *J. Hydrol.* **320**, 18–36 (2006).
- 795 50. Reisinger, D. & Füllsack, M. Comparing Equation-Based and Agent-Based Data Generation
796 Methods for Early Warning Signal Analysis. *Syst. 2020, Vol. 8, Page 54* **8**, 54 (2020).
- 797 51. Scheffer, M. *et al.* Early-warning signals for critical transitions. *Nature* **461**, 53–9 (2009).
- 798 52. Bury, T. M. *et al.* Deep learning for early warning signals of tipping points. *Proc. Natl. Acad.*
799 *Sci. U. S. A.* **118**, (2021).
- 800 53. Doncaster, C. P. *et al.* Early warning of critical transitions in biodiversity from compositional
801 disorder. *Ecology* **97**, 3079–3090 (2016).
- 802 54. Wang, R. *et al.* Network parameters quantify loss of assemblage structure in human-
803 impacted lake ecosystems. *Glob. Chang. Biol.* **25**, 3871–3882 (2019).
- 804 55. Mayfield, R. J. *et al.* Metrics of structural change as indicators of chironomid community
805 stability in high latitude lakes. *Quat. Sci. Rev.* **249**, 106594 (2020).
- 806 56. Cai, Y., Lenton, T. M. & Lontzek, T. S. Risk of multiple interacting tipping points should
807 encourage rapid CO2 emission reduction. *Nat. Clim. Chang.* **2016 65 6**, 520–525 (2016).
- 808 57. Dietz, S., Rising, J., Stoerk, T. & Wagner, G. Economic impacts of tipping points in the climate
809 system. *Proc. Natl. Acad. Sci. U. S. A.* **118**, (2021).
- 810 58. Fabbri, S., Hauschild, M. Z., Lenton, T. M. & Owsianiak, M. Multiple climate tipping points
811 metrics for improved sustainability assessment of products and services. *Environ. Sci.*
812 *Technol.* **55**, 2800–2810 (2021).
- 813 59. Steffen, W., Broadgate, W., Deutsch, L., Gaffney, O. & Ludwig, C. The trajectory of the
814 Anthropocene: The Great Acceleration: *Anthr. Rev.* **2**, 81–98 (2015).
- 815 60. R Core Team. R: A language and environment for statistical computing. at [https://www.r-](https://www.r-project.org/)
816 [project.org/](https://www.r-project.org/) (2020).

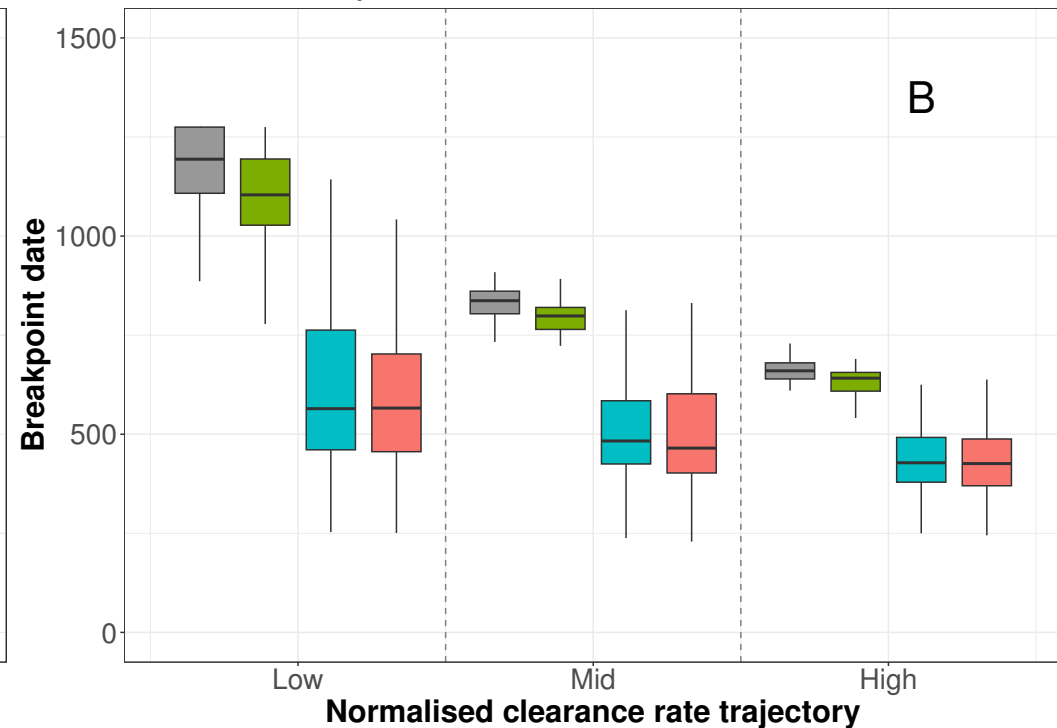
- 817 61. Carpenter, S. R. Eutrophication of aquatic ecosystems: Bistability and soil phosphorus. *Proc.*
818 *Natl. Acad. Sci. U. S. A.* **102**, 10002–10005 (2005).
- 819 62. Rheinboldt, W. C. Methods for Solving Systems of Nonlinear Equations. *Methods Solving Syst.*
820 *Nonlinear Equations* (1998) doi:10.1137/1.9781611970012.
- 821 63. Huang, S., Zhang, K., Lin, Q., Liu, J. B. & Shen, J. Abrupt ecological shifts of lakes during the
822 Anthropocene. *Earth-Science Rev.* **227**, 103981 (2022).
- 823 64. IPCC. Climate Change 2013: The Physical Science Basis. in *Contribution of Working Group I to*
824 *the Fifth Assessment Report of the Intergovernmental Panel on Climate Change* (eds. Stocker,
825 T. F. et al.) 1535 (Cambridge University Press, 2013).
- 826 65. Worm, B. *et al.* Rebuilding Global Fisheries. *Science (80-.)*. **325**, 578–585 (2009).
- 827 66. Pinsky, M. L., Jensen, O. P., Ricard, D. & Palumbi, S. R. Unexpected patterns of fisheries
828 collapse in the world’s oceans. *Proc. Natl. Acad. Sci. U. S. A.* **108**, 8317–8322 (2011).
- 829 67. Drijfhout, S. *et al.* Catalogue of abrupt shifts in Intergovernmental Panel on Climate Change
830 climate models. *Proc. Natl. Acad. Sci. U. S. A.* **112**, E5777–E5786 (2015).
- 831 68. Zeileis, A., Leisch, F., Hornik, K. & Kleiber, C. Package “strucchange”. [https://cran.r-](https://cran.r-project.org/web/packages/strucchange/strucchange.pdf)
832 [project.org/web/packages/strucchange/strucchange.pdf](https://cran.r-project.org/web/packages/strucchange/strucchange.pdf) (2015).
- 833 69. Wickham, H. ggplot2: Elegant Graphics for Data Analysis. at [https://doi.org/978-3-319-24277-](https://doi.org/978-3-319-24277-4)
834 [4](https://doi.org/978-3-319-24277-4) (2016).
- 835



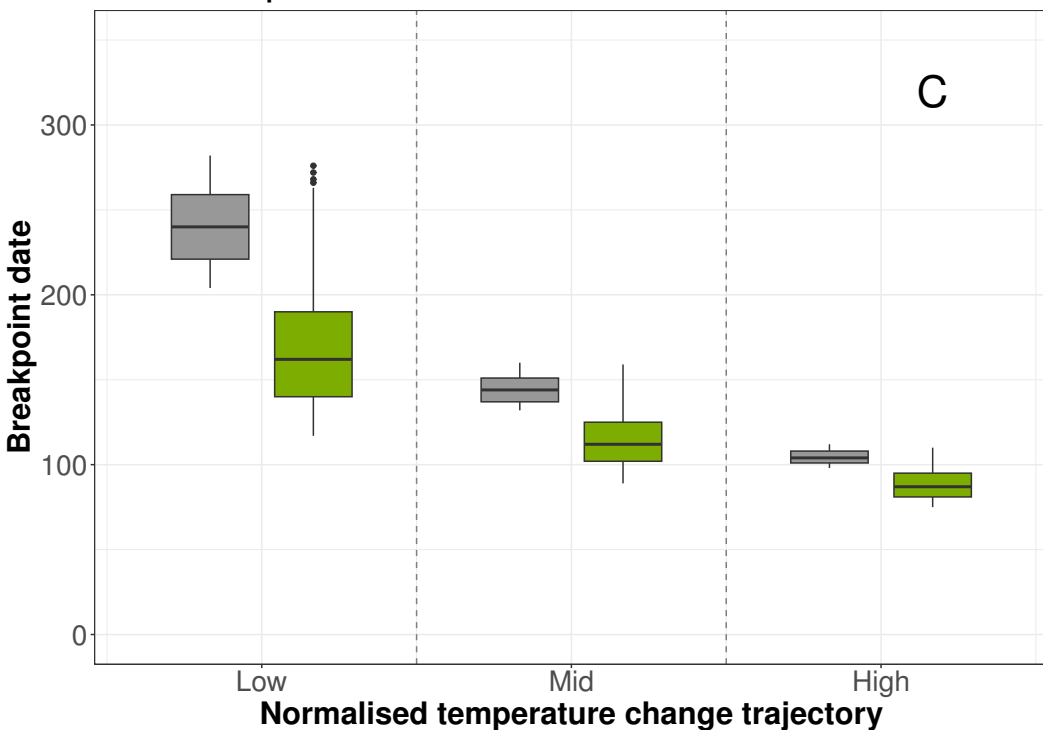
Lake Chilika: Multiple slow rates



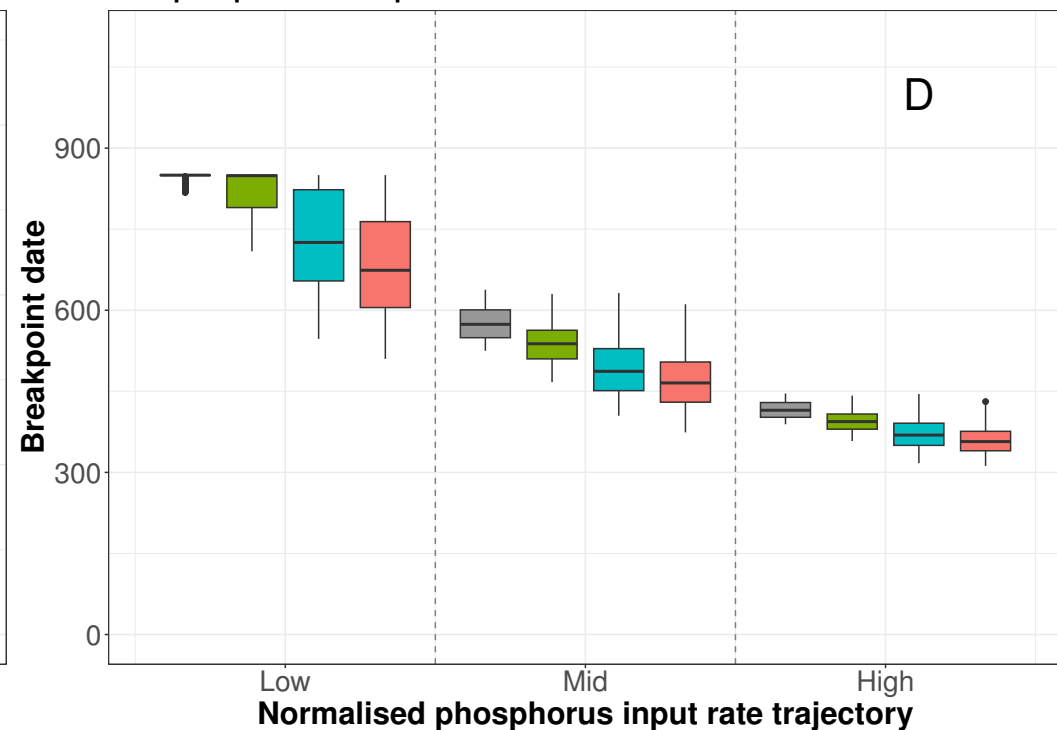
Easter Island: Multiple slow rates



TRIFFID: Multiple slow rates

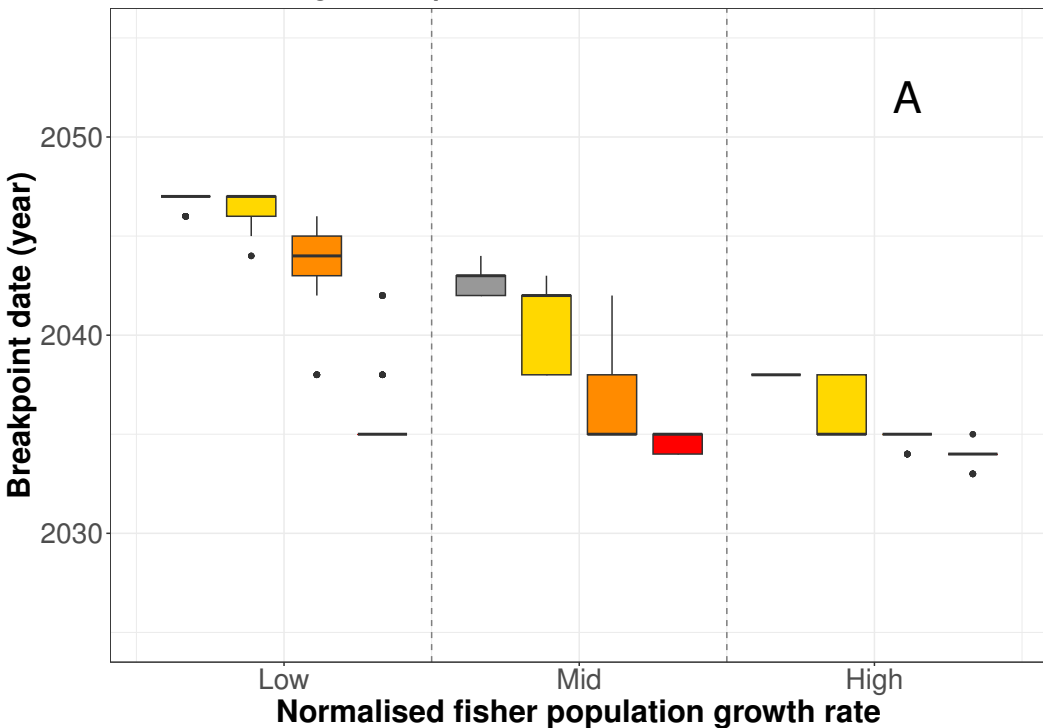


Lake phosphorus: Multiple slow rates

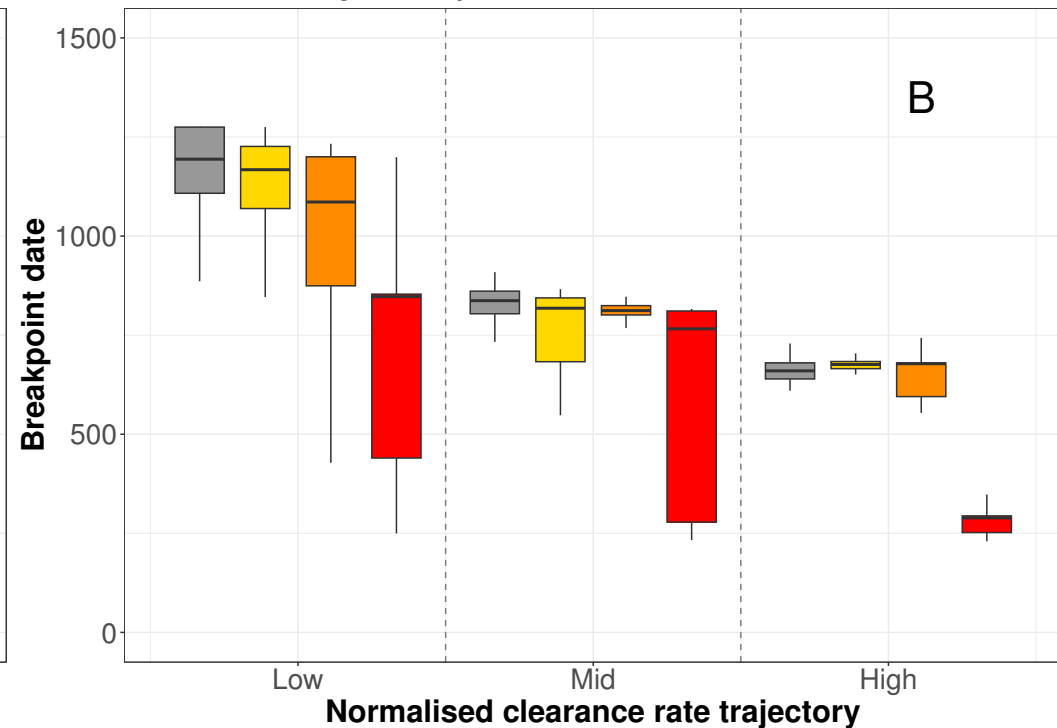


Scenario Baseline Secondary Tertiary All

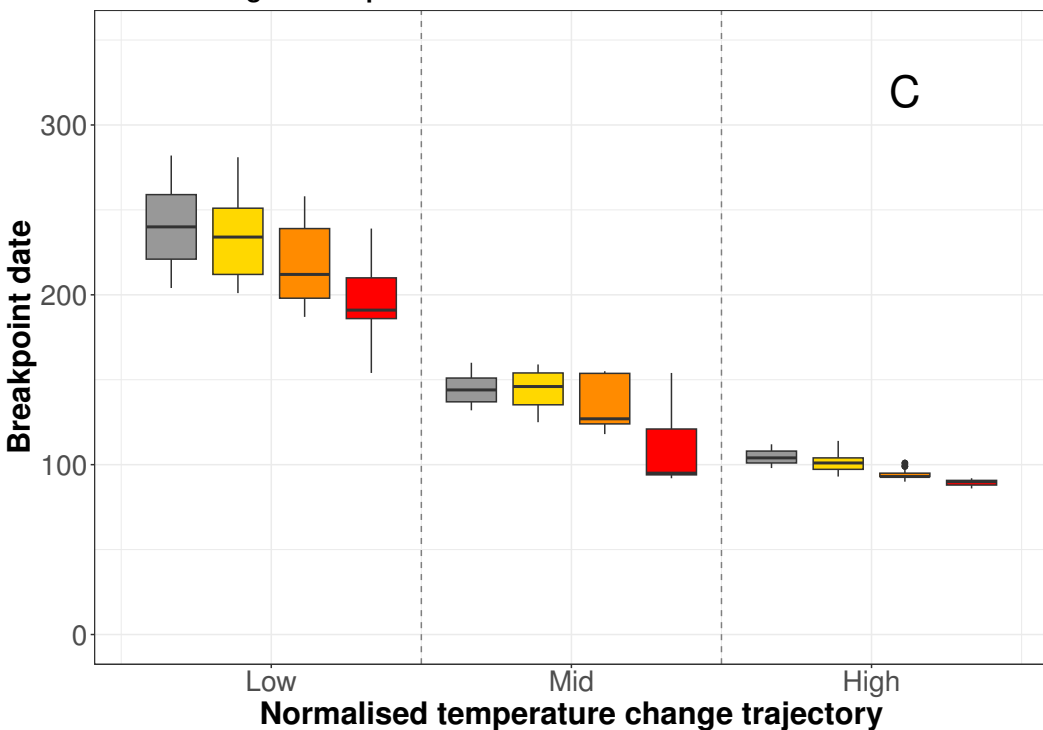
Lake Chilika: Single uncoupled noise



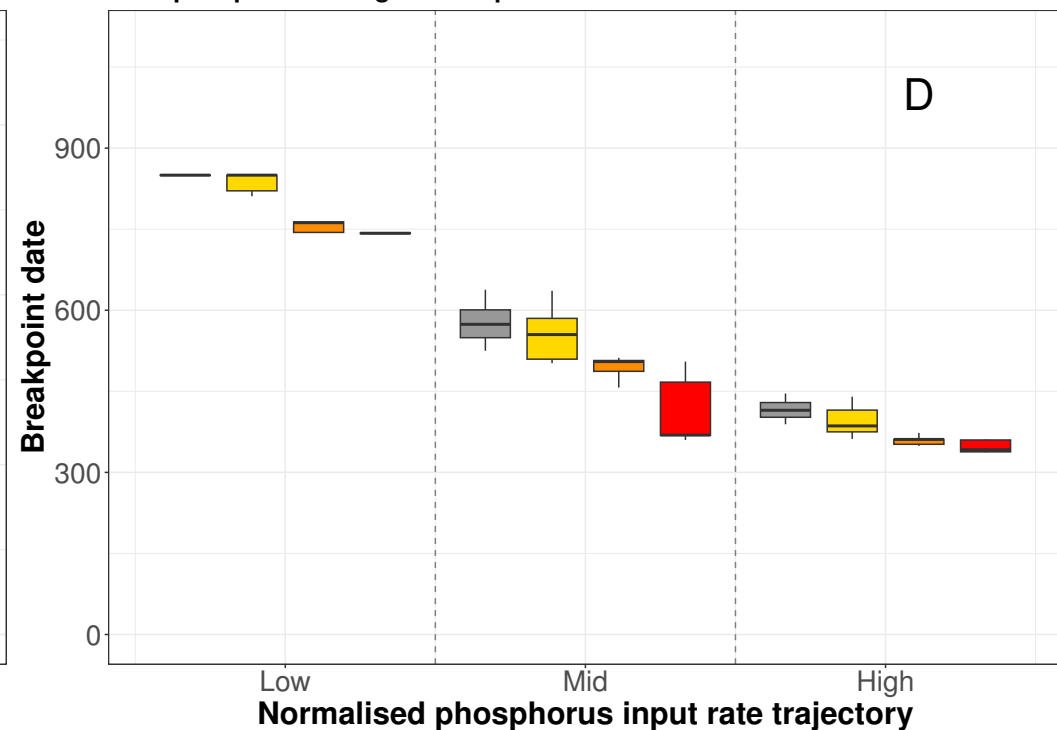
Easter Island: Single uncoupled noise



TRIFFID: Single uncoupled noise

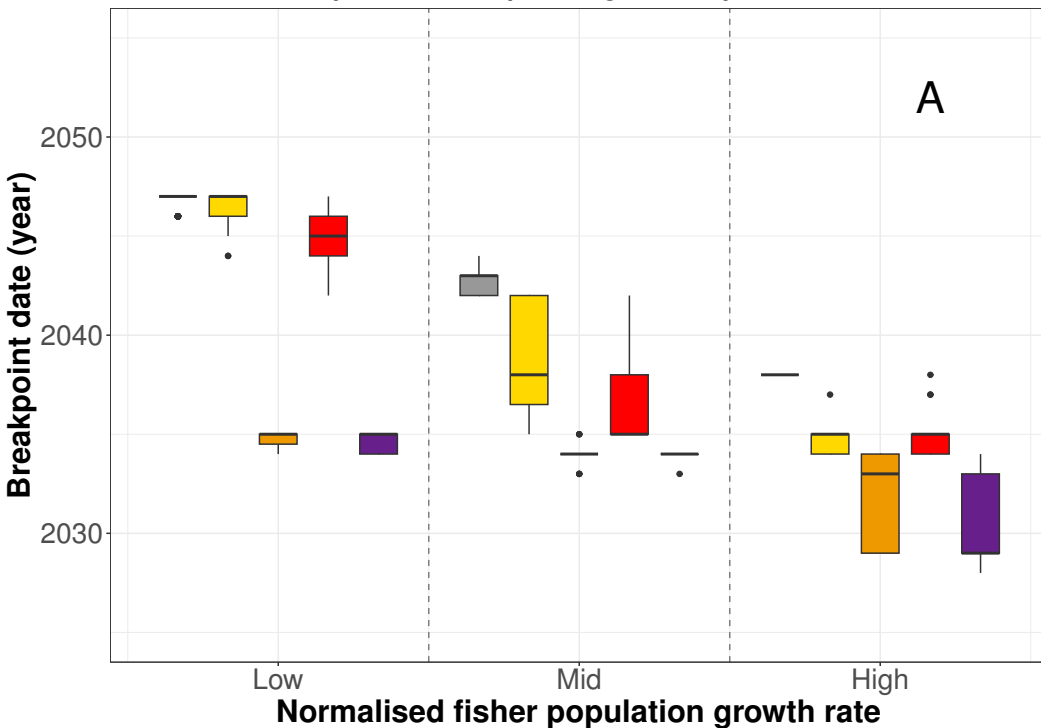


Lake phosphorus: Single uncoupled noise

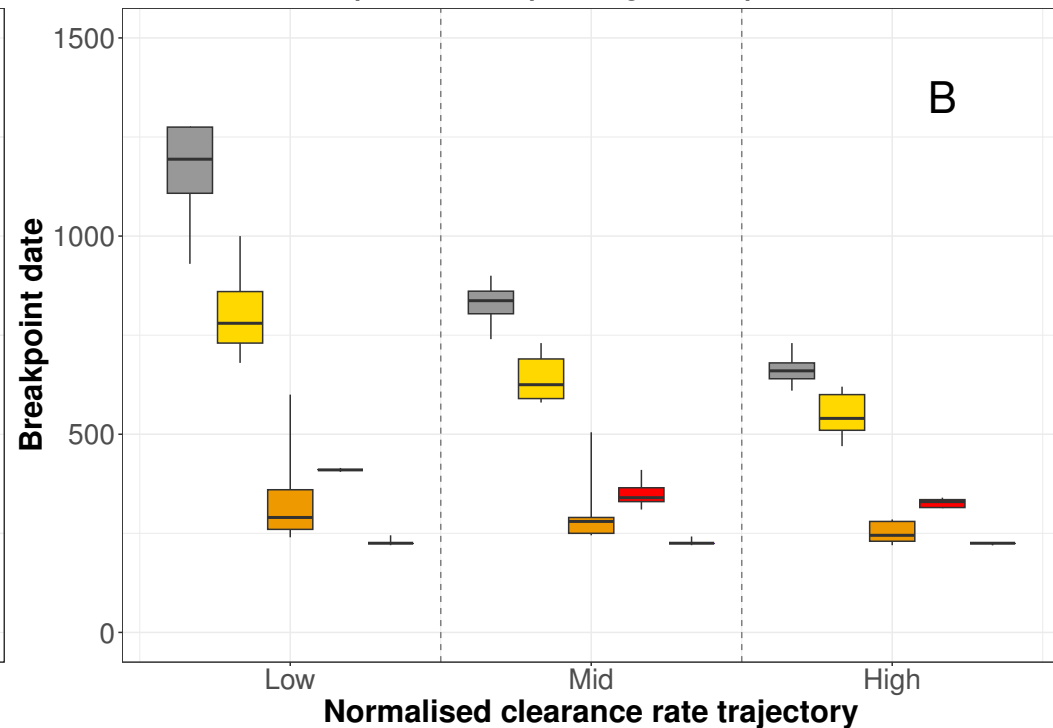


Noise ■ Baseline ■ Low ■ Mid ■ High

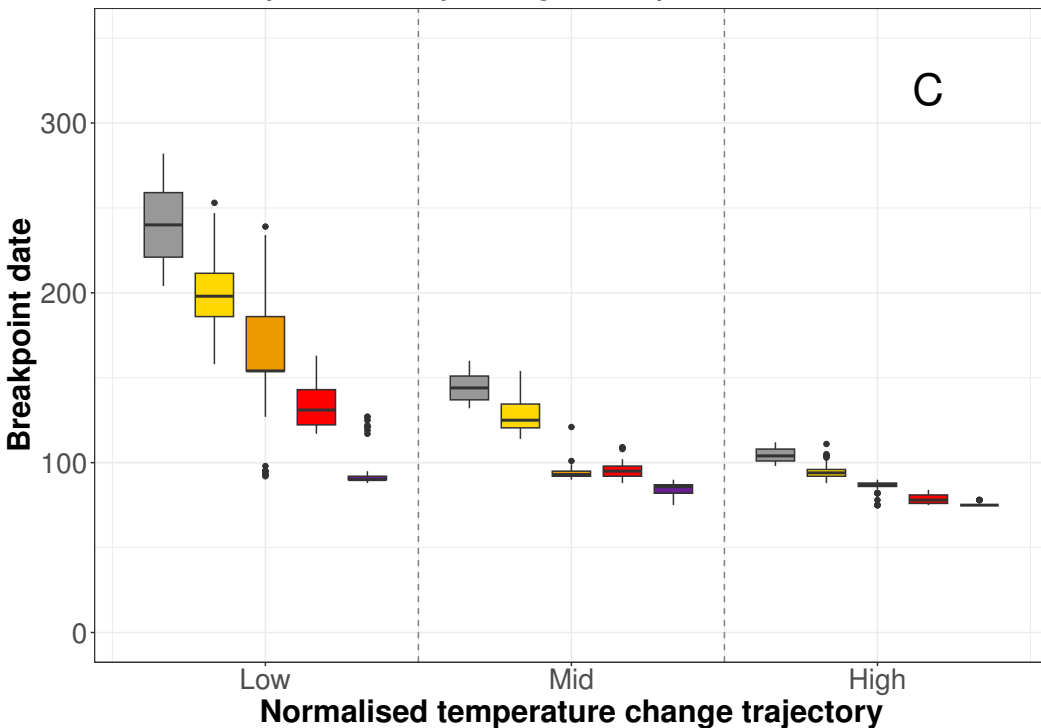
Lake Chilika: Multiple slow rates plus single uncoupled noise



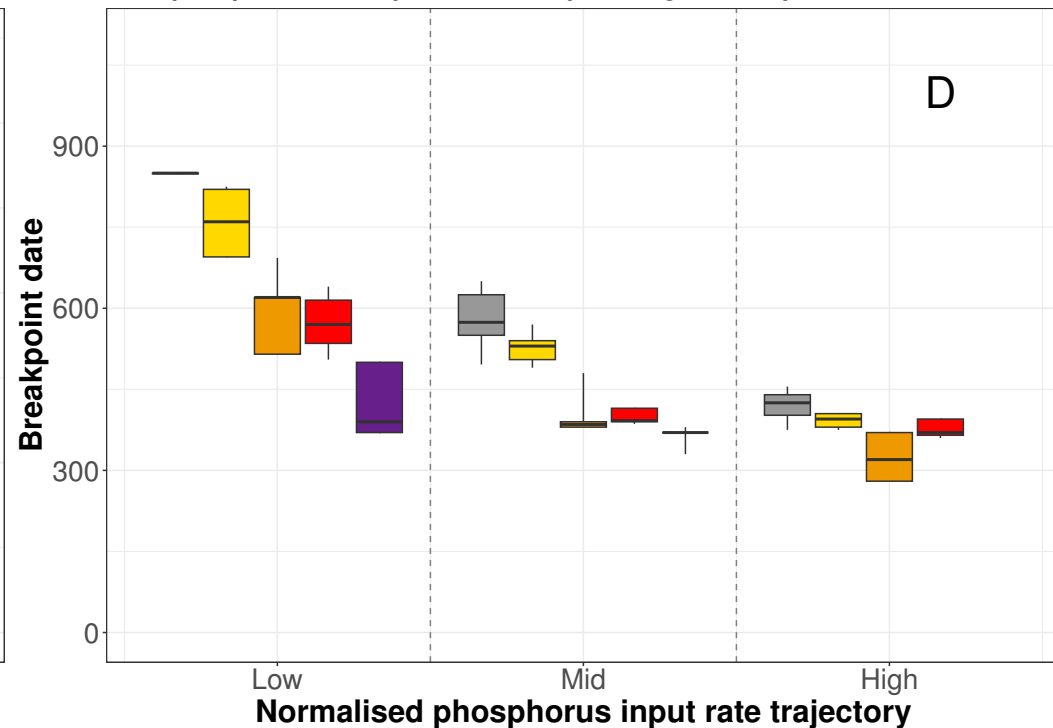
Easter Island: Multiple slow rates plus single uncoupled noise



TRIFFID: Multiple slow rates plus single uncoupled noise



Lake phosphorus: Multiple slow rates plus single uncoupled noise



Combination Baseline Low T, Low N Low T, High N High T, Low N High T, High N